JOURNAL OF MATERIALS SCIENCE 10 (1975) 669-682

Frank's kinematic theory of crystal dissolution applied to the prediction of apex angles of conical ion-bombardment structures

M. J. WITCOMB
Electron Microscope Unit, University of the Witwatersrand, Johannesburg, South Africa

The construction process associated with the kinematic theorems of crystal dissolution due to Frank has been applied to the problem of determining the characteristics of surface topography caused by ion bombardment. Such an approach is shown to be valid by comparison between experimental results on and dissolution constructions applied to ion-etched spheres. Emphasis has been placed on determining the apex angle of equilibrium cone structures on crystalline materials. The values predicted for the apex angle by Frank's method have been found in good agreement with those measured experimentally and values derived from the peak of sputter yield curves or from ion channelling calculations. Using different starting shapes, the importance is stressed of ensuring the presence of adequate orientation directions without which only non-equilibrium dome type structures or pseudo-cones will develop.

1. Introduction

Barber *et al.* [1] have shown how semiquantitatively Frank's kinematic theory of chemical dissolution of crystals [2, 3] can be used to determine the development of surface topographies on materials subject to ion bombardment. More recently, Carter *et al.* [4] have emphasized the importance of the slowness of erosion curve used in this construction process. In particular, they have pointed out that when a cone-shaped structure develops, the cone apex angle is related to $\pm\,\theta_m$ where θ_m is the angle of incidence of the ion beam to the target surface for which the normals to the slowness of erosion curve are parallel to the $\theta = 0$ axis in the polar diagram. It can be shown that θ_m is equal to the angle corresponding to the peak in the sputter yield curve. This peak angle is generally denoted by the symbol θ_p or $\hat{\theta}$ and is known to be a function of target material and both type and energy of the bombarding ion. Experiment and calculation [4, 5] have indicated that $\hat{\theta}$ is related to the cone apex angle α_c through the relation

$$\alpha_c = 180^\circ - 2\hat{\theta}. \qquad (1)$$

It must be noted that it is possible for a cone to develop for which the apex angle is independent of $\hat{\theta}$ [6]. The conditions under which this can occur are probably less likely to be found in practice especially in the case of materials having second phase particles in or on their surface. Reference will, however, be made to such cones later.

The object of the present work was to determine the accuracy to which one might predict, using the Frank construction, profiles of ion-etched crystalline materials and in particular the equilibrium apex angles of surface cones. The latter values will be compared with those obtained using Equation 1 and calculations based on ion channelling [7]. In order to derive this information, a selection of published sputter yield curves representative as far as possible of a wide cross-section of targets and bombarding ions have been collected from the literature. The reason that the energy range considered is essentially restricted to the 0.2 to 1.05 keV region for all elements excepting copper is due solely to a lack of suitable data. Each set of sputter yield data has then been applied to an erosion construction as laid down in the paper of Barber *et al.* [1]. Only construction details particular to the etching of present structures or guidelines

© *1975 Chapman and Hall Ltd.*

considered useful for checking accuracy will be discussed here. Since cones with apex angles related to the peak of the sputter yield curve are the centre of interest in this paper, all initial shapes will contain the orientation corresponding to $\hat{\theta}$.

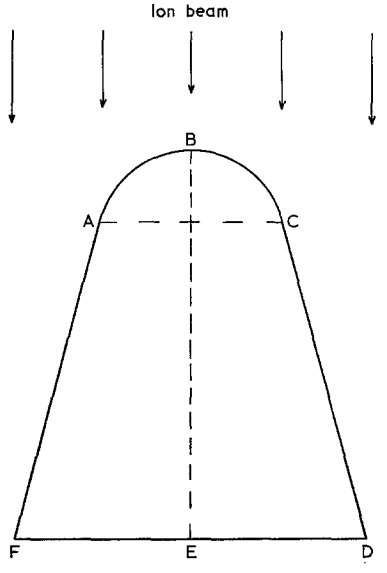

Figure 1 Schematic diagram of the standard structure.

2. Configuration and construction process

The configuration chosen in the present study is schematically illustrated in Fig. 1 and is from hereon referred to as the standard structure. It represents a two-dimensional view of a three-dimensional object which is symmetrical about the axis BE. The end ABC of the structure is positioned to face an ion beam collimated parallel to this axial direction. To achieve uniform etching, it is necessary for the beam diameter to be greater than the distance DF. In two dimensions the area ABC is a segment of a circle. The diameter of the circle from which the segment was taken was generally 25.4 cm. While smaller diameters have been tried, with considerable success, such as 15 cm in Figs. 6 and 7, and 10 cm, the significant inaccuracies experienced in a few cases was felt to probably justify the use of the larger dimensions whenever practicable. The area ACDF is a trapezium, the sides AF and CD of which are tangential to the segment ABC at A and C respectively. Such a shape was chosen for the following reasons. Firstly, since ABC is a part of a circle, this region of the initial shape can conveniently be made from polar graph paper. Angles and orientation directions are then easily obtainable at any time during the Frank construction process. In addition, the positioning of the sides AF and CD is flexible in order to allow the important stabilizing orientation directions to be present within the structure at least up to the point when an equilibrium cone configuration develops. In practice, this means that the two orientation directions AF and CD are tied to the $\hat{\theta}$ value. The criteria used in the present case was that if point B corresponds to 0° orientation then points A and C should occur at an angle at least equal to or greater than $\pm(\hat{\theta} + \theta')$ where θ' is inversely proportional to $\hat{\theta}$. In practice, a small $\hat{\theta}$ value implies highly divergent orientation trajectories so that θ' must be large for the trajectories corresponding to $\pm(\hat{\theta} + \theta')$ to enclose all necessary trajectories. Typical values are $\hat{\theta} = 38°$, $\theta' = 32°$; $\hat{\theta} = 70°$, $\theta' = 14°$. The larger the $(\hat{\theta} + \theta')$ value, the closer the segment of circle at the top of the structure approaches a semicircular shape, so representing a hemisphere in three dimensions. If the boundary lines AF and CD do not enclose sufficient orientation trajectories, a false value for the equilibrium cone angles will ensue. The importance of this point will be emphasized later. It should be noted at this stage that the term "equilibrium" in this paper refers to the condition where a cone shape has developed and the apex angle α_c then remains constant until all the cone material is etched away if the conical shape is formed on a second phase particle or until a flat perpendicular to the ion-beam direction is developed if the cone results from a surface contour on a single phase material. The movement of the conical face with etching time in a direction parallel to the ion beam is not important for present considerations as long as the α_c value does not change.

The height BE of the initial structure, Fig. 1, is taken in practice to be sufficiently variable to allow a completely equilibrium conical configuration to develop. Such an arrangement is necessary since the establishment of a true equilibrium conical structure can require the removal of a considerable amount of material from the bombarded profile [6, 8, 9]. This situation is frequently not attained in real experiments, the ion etched metal spheres of Wehner being a case in particular. The speed

with which an equilibrium shape forms will be dependent not only on the starting profile of the target but also on such factors as type and crystal orientation of the target material, species and energy of the bombarding ion, and poisoning ratio caused by the presence of gaseous impurities [10].

In the present constructions, a reasonable equilibrium-like ion-bombardment shape was generally achieved after etching away an axial length of about $8d$ where d is the diameter of the circle from which the top curved surface was taken. Although such large distances are awkward, considerable advantages were considered to be derived from the above dimensions. In particular, the relatively large diameter of the top segment ABC yields an acceptable length of arc per angle interval of initial circumference. This is important since the relevant portion of the slowness of erosion curve for true equilibrium structures is that corresponding to the sputter yield curve at angles greater than $\hat{\theta}$, an area where the projected separation per unit angle of initial curved surface onto the axis perpendicular to the ion beam (AC) decreases rapidly with increasing angle. Since the orientation trajectories are close together, see Fig. 2, and experimental errors are more significant in this region, precise trajectory positioning is imperative. In addition, a large slowness of erosion curve is also beneficial as the curvature of this is generally only changing slowly for $\theta > \hat{\theta}$ so that considerable errors can be incurred in the determination of the directions of the orientation trajectories.

Before discussing results, it is perhaps worthwhile noting a few points on the construction process and sputter yield data to be considered. Firstly, a helpful indicator to the accuracy of the erosion curve is that at the orientation $\hat{\theta}$, $dS/d\theta = 0$. This acts as useful information to feed back to the erosion curve and modify it if necessary once a few orientation trajectories have been drawn either side of the $\hat{\theta}$ trajectory. In the present investigation the positioning of the $\hat{\theta}$ trajectory could at least be made to within the area which should be bounded by $\mathrm{tr}(\hat{\theta} \pm 0.5°)$ where $\mathrm{tr}(\theta)$ denotes a trajectory associated with an orientation θ on the original surface. Secondly, in the final step of the Frank construction process, the distance to be side-stepped is in a direction perpendicular to the edges of the parallel rules and not in the direction of the trajectory. Lastly, due to Wehner's particular

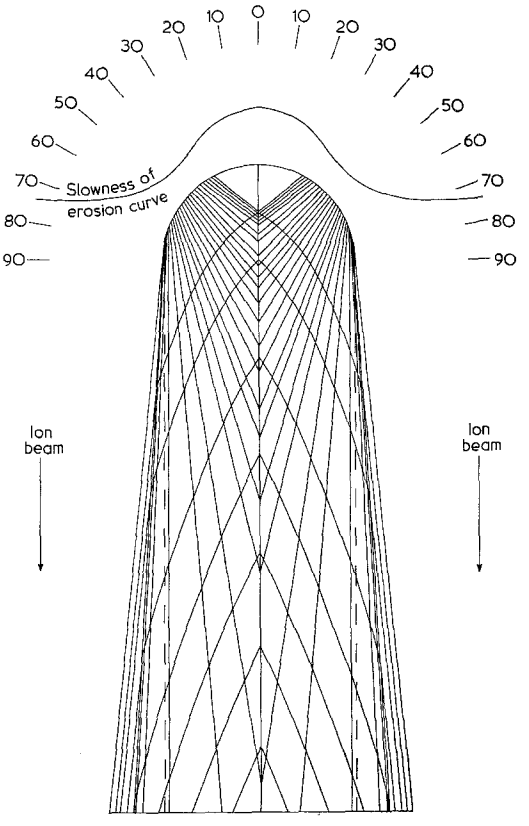

Figure 2 Polar diagram of the slowness of erosion curve, dissolution trajectories and derived profiles of a copper standard structure etched by 2.05 keV argon ions.

procedure for plotting the sputter yield curve, it has been necessary in order to obtain yield values perpendicular to the surface to multiply his yield data by $\cos\theta$ so that the slowness of erosion curve is given by the function $S(0)/[S(\theta)\cos^2\theta]$ where $S(0)$ and $S(\theta)$ are respectively the sputter yield values at normal ion incidence and at an angle $90° - \theta$ to the specimen surface.

3. Results and discussion

3.1. Standard structure and calculations

Typical examples of a Frank construction applied to a standard structure are illustrated in Figs. 2 and 3 where etch profiles are shown corresponding to distances down the vertical axis of $0.25d$, $0.5d$, then by intervals of $0.5d$ to $3d$.

Fig. 2 is constructed from the data of Oechsner [11] for 2.05 keV argon ions incident on a copper target and is meant to be representative of profile development resulting from high energy

bombardment. Trajectories are shown every 2° from 28° to 84°, the latter orientation corresponding to the point where the tangent has been drawn to the top curved surface to give sides to the structure. For clarity, trajectories corresponding to angles smaller than 28° have been omitted.

After the initial intersections of the lower angle orientation trajectories, a dome-type structure is clearly in evidence (Fig. 2). Such an intermediate shape has been observed to develop on ion-bombarded precipitates in stainless steel [12, 13]. The extent to which the dome-like profile is pronounced is dependent upon the atomic number of the target atoms and upon the atomic number and energy of the incident ion. This shape becomes a less marked feature as ion energy decreases and/or the ion mass increases, for example, see Figs. 3 and 7. While the dome-type topography remains for a considerable period of etching it becomes less prominent with time and finally changes into the equilibrium cone configuration with a particular apex angle. Once this development has occurred,

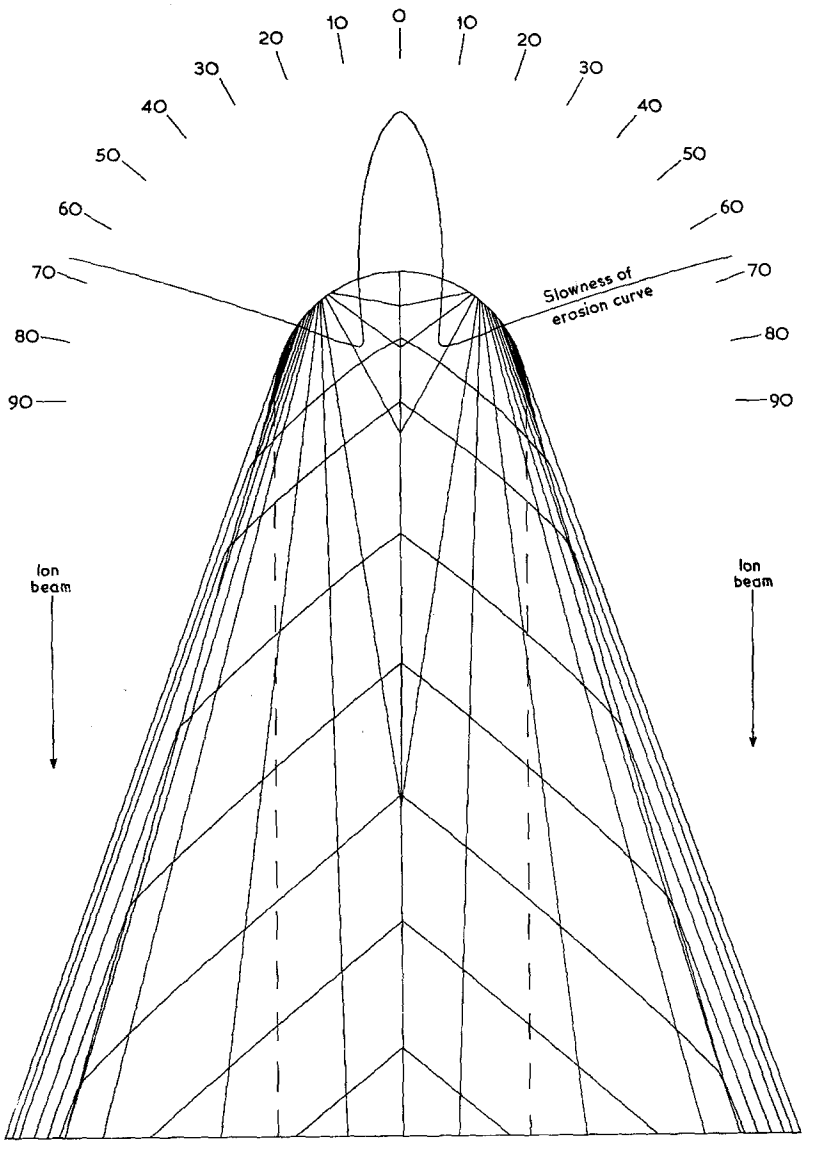

Figure 3 Polar diagram of the erosion of a molybdenum standard structure by 0.2 keV mercury ions.

TABLE I

Target material	Z_2	Z_1	keV	$0.25d$	$0.5d$	d	$2d$	$3d$	$(\alpha_c)_M$	Ref.
Cu	29	18	2.05	110	93	66	50	46	40	[11]
Mo	42	80	0.2	117	107	104	101	101	100	[14]

the characteristic cone angle will remain constant as further etching simply causes the material to recede in the direction BE. To indicate the speed with which the equilibrium apex angle is approached, Table I lists the angle at the apex region of etching profiles which has been measured on the present constructions at different etching distances down the structure axis. The values listed under $(\alpha_c)_M$ are the values obtained by substituting the $\hat{\theta}$ value from the appropriate sputter yield curve into Equation 1. It can be seen that considerable material must be etched away to achieve an equilibrium conical state. This is rather more so than implied by the values in Table I since these only reflect the angle in the vicinity of the apex and ignore the rest of the profile curvature. At the $3d$ point, orientation trajectories covering the range 66° to 70° still have to be removed before a true equilibrium cone profile can be expected to emerge [4]. An example of an intermediate stage in Fig. 2 is illustrated in the scanning micrograph, Fig. 4. This shows a MnS inclusion left standing proud of an extruded 18-8 stainless steel matrix after etching by 0.3 keV argon ions incident perpendicular to the matrix surface.

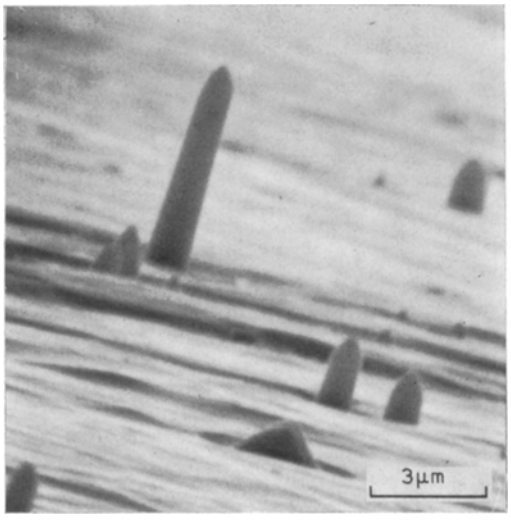

Figure 4 An intermediate ion etching profile of a standard structure-like MnS inclusion emerging from a stainless steel target.

The low energy etching profile changes are illustrated in Fig. 3. This diagram is constructed from the data of Wehner [14] for 0.2 keV mercury ions incident on a molybdenum target. Except for the addition of tr(39°), trajectories are shown every 2° from 32° to 70° inclusive. Structure sides are derived from tangents at the orientation 70° on the top curved face. No trajectories are marked below 32° as they are too close together for the scale of the figure and really add nothing to the diagram. Comparing Figs. 2 and 3 it is evident that the combination of lower energy and high atomic number of the ion produces a slowness of erosion curve showing marked curvature changes. This results in much earlier elimination of the lower angle trajectories which together with the greater divergence of trajectories either side of tr($\hat{\theta}$) cause the early establishment of the equilibrium conical face. The influence of the sputter yield curve on trajectory spacing and profile changes will be discussed in detail in Section 3.3. Low ion energies encourage larger cone apex angle so that, as a result, in Fig. 3 dome-type profiles are only really noticeable down as far as the $0.5d$ position and any curvature on the conical profile face is practically lost at the $2d$ mark. The latter is emphasized by the angles measured at the apex region for different etching distances listed in Table I.

Slight modifications not shown here can occur to a conical structure during the erosion process if it is near another structure such that ions reflected from either structure can etch away areas of the other. This situation could occur for instance in the case of ion etching of a matrix material containing second phase particles. In addition, ions reflected off the sides of a cone can cause a groove to develop in the matrix material surrounding the base of the cone [5, 13]. More recently, Sigmund has discussed "downstream" effects caused by locally oblique ion incidence [15]. None of these effects are taken into account, however, by the Frank construction since this

was formulated for chemical etching processes where ion reflection is not applicable.

The true equilibrium cone angle values determined from constructions similar to Figs. 2 and 3 are listed under the column heading $(\alpha_c)_{FS}$ in Tables II and III for differing materials and experimental conditions. The $(\alpha_c)_{FS}$ values obtained from Frank constructions can be seen to be in excellent agreement with the $(\alpha_c)_M$ values. The divergence between the two sets of apex angles is easily within the experimental error of up to about 5° typically experienced. This agreement is pleasing since the distances involved in the present construction might have been expected to lead to significant discrepancies. The above results thus imply that Frank's construction process can be used with reasonable confidence to determine the apex angle of equilibrium cone structures on ion-etched surfaces. In addition, considerable reliability can now be placed on the intermediate topography profiles predicted by this method. Such comments are given further weight in the next section on the ion bombardment of spheres.

Recent calculations have shown that the cone apex angle of ion-etched crystalline materials can also be predicted from ion channelling calculations using the equation [7]

$$\alpha_c = \frac{134}{d(Z_1^{\frac{2}{3}} + Z_2^{\frac{2}{3}})^{\frac{1}{2}}} \left[\frac{Z_1 Z_2 (Z_1^{\frac{2}{3}} + Z_2^{\frac{2}{3}})^{\frac{1}{2}}}{n^{\frac{1}{3}} E}\right]^{\frac{1}{4}}. \quad (2)$$

Z_1 and Z_2 are, respectively, the atomic numbers of the incident ion and target atoms, n is the number of atoms per unit cell of target material, E is the ion energy in electron volts, and d is the target atom spacing taken to be the close-packed atom separation unless known to be otherwise. Both d and n are in Ångstrom units. A concept such as channelling is not unreasonable at low ion energies. For example, at 0.5 keV, while normal penetration by incident ions is in the range 5 to 10 Å, it is known that in the extreme energy can be transmitted for about 100 atomic distances along a close-packed direction [18].

The cone angles derived from Equation 2 are given in the column headed $(\alpha_c)_C$ in Tables II and III. It can be seen at least for the conditions considered here that the construction process and calculation procedure yield equally acceptable results. The Frank construction yields the cone apex angle to within an average deviation of about 5% compared to the values obtained from Equation 1, while Equation 2 predicts α_c to within 8%. If the case of helium bombardment is neglected due to larger than normal scatter in the experimental points these figures become 4% and 7% respectively. Of course, while the calculation procedure shortcuts the need for yield data and the drawing of a Frank diagram, it does require precise details of the target's composition, crystallinity and ion channelling direction appropriate to each case. If the latter is unknown,

TABLE II

Target material	Z_2	keV	$(\alpha_c)_{FS}$	$(\alpha_c)_M$	$(\alpha_c)_C$	Ref.
Al	13	1.05	41	39	38	[11]
Pd	46	1.05	58	59	50	[11]
Ta	73	1.05	49	50	54	[11]
Fe*	26	0.8	73	73	68	[14]
W*	74	0.8	80	85	82	[14]
Mo*	42	0.2	99	100	105	[14]

All bombarded by Ar ($Z_1 = 18$) except those marked by * where Hg ($Z_1 = 80$) was used.

TABLE III

Bombarding ion	Z_1	keV	$(\alpha_c)_{FS}$	$(\alpha_c)_M$	$(\alpha_c)_C$	Ref.
Xe	54	30.0	23	20	25	[16]
Ar	18	27.0	22	24	21	[17]
Xe	54	9.5	35	31	34	[16]
Xe	54	1.05	57	59	59	[11]
Kr	36	1.05	47	49	54	[11]
Ar	18	1.05	44	45	47	[11]
He	2	1.05	32	38	28	[11]
Xe	54	0.55	67	68	69	[11]

Target material Cu ($Z_2 = 29$).

the atom spacing along the close packed direction appears to be adequate in most cases [7]. The advantage of the Frank construction is that it would seem to be capable of evaluating the intermediate topographical changes accurately if these are so desired.

TABLE IV

Bombarding ion	Z_1	$\mathrm{tr}(\theta_p - 1°)$
Xe	54	$18d$
Kr	36	$37d$
Ar	18	$53d$
He	2	$70d$

Target material Cu ($Z_2 = 29$). Ion energy 1.05 keV.

It has been mentioned in Section 2 that it is important when trying to predict the characteristics of equilibrium cone configurations to ensure that the relevant orientation trajectories remain present within the structure. A truly equilibrium conical shape finally develops when all material embodying orientation trajectories less than $\mathrm{tr}(\hat{\theta})$ are eliminated [4]. Rough estimates of the point at which $\mathrm{tr}(\hat{\theta} - 1°)$ crosses the vertical structure axis and is lost, have been estimated from the construction diagrams and are given in Table IV for bombardment of copper by different species of 1.05 keV ions. This shows, as mentioned earlier, that a considerable amount of material is sometimes needed to be etched away in order to achieve the complete elimination of this orientation trajectory and result in the formation of a true equilibrium shape. If, however, sufficient material has not been removed so that $\mathrm{tr}(\hat{\theta} - \theta)$ is still present where θ is in the order of a few degrees, a pseudo-conical profile can be obtained. Such a profile can be said to exist when trajectories for angles less than $\hat{\theta}$ are included but for all intents and purposes the slight curvature on the profile is insignificant or indistinguishable. A typical example is that of 1.05 keV Xe^+ bombardment of Cu which yields after $4.3d$ of axial etching a pseudo-cone. This structure has an apex angle of 61°, a value deviating only 2° from $(\alpha_c)_M$ and $(\alpha_c)_C$. Although under these experimental conditions $\hat{\theta} = 60.5°$, the orientation trajectories utilized to derive the above value were those covering the range 57° to 76°. Such behaviour is even more marked when the low energy data due to Wehner covering the range 0.2 to 0.4 keV bombardment is used. Generally in this case, very large amounts of etching are required to achieve true equilibrium and this is why most $(\alpha_c)_{FS}$ values have not been given in Table II. Pseudo-cone shapes, however, occur early, see Tables I and V. Reducing the scale of the diagram does not help since the greater difficulty in trajectory positioning causes further errors which are then magnified over large axial distances. As indicated above and from Fig. 2, the final approach to a true equilibrium cone shape may, in most cases, be academic. For example, an experimentalist viewing etch profile changes *in situ* in a typical scanning electron microscope, within the limits of the available viewing angle and of the instrument's resolution, may well observe a condition like equilibrium to occur much earlier than indicated here. Such an instrument limitation should not stop the person from observing at least the main intermediate profile changes and achieving a reasonable value for the equilibrium apex angle.

TABLE V

Target material	Z_2	keV	$(\alpha_c)_M$	$(\alpha_c)_{FC}$ at $0.85d$	$(\alpha_c)_{FR}$				
					at $0.85d$	at $1d$	at $2d$	at $4d$	Ref.
Al	13	1.05	39	69	55	55	48	47	[12]
Pd	46	1.05	59	82	69	69	65	61	[12]
Ta	73	1.05	50	74	63	60	58	53	[12]
Fe*	26	0.8	73	76	75	75	74	74	[13]
W*	74	0.8	85	89	85	85	83	82	[13]
Fe*	26	0.4	80	82	82	82	80	80	[13]
W*	74	0.4	80	84	82	82	80	80	[13]
Ni*	28	0.2	97	102	100	100	100	98	[13]
Mo*	42	0.2	100	106	104	104	101	101	[13]
W*	74	0.2	94	116	106	106	100	97	[13]

All bombarded by Ar ($Z_1 = 18$) except those marked by * where Hg ($Z_1 = 80$) was used.

In practice, one is not always at liberty to choose the starting shape of the structure to be ion bombarded, for example, second phase particles in a metal or alloy specimen. To gauge the effect of so-called non-ideal shapes, two typical simple forms have been taken for study. The first, a sphere, generalizes the shape of many inclusions resulting from phase changes or impurity precipitation occurring on heat-treatment of materials or from substances added as killing agents to steel [13]. The two-dimensional Frank construction on a sphere will also image the change in cross-section of a rod or fibre etched at right angles to the long axis. The second form to be considered is that of a fibre or rod with a hemispherical end, the ion-beam direction being parallel to the long axis of the rod. This shape might represent single fibres in a fibre composite or precipitates in an extruded matrix. The following will describe in some detail the topographic changes on ion etching spheres and rods with particular emphasis placed on developing conical shapes. Mention is first made, however, of the effects of points of inflexion which were found to be features occurring in both the high- and low-angle regions of the slowness of the erosion curve.

3.2. Inflexion points in the erosion curve

In the paper by Carter *et al.* [4], the slowness of erosion curve is shown with an upward concavity from $\hat{\theta}$ to at least θ^x where $S(\theta^x) = S(0)$. Present work has indicated a point of inflexion to exist in the curve in this orientation range. Since the curve is rising immediately after $\hat{\theta}$, such a point must exist as the curve has to have a downward slope to satisfy the condition

$$\lim_{\theta \to 90^\circ} = \frac{S(0)}{S(\theta)\cos\theta} = 0 .$$

The main properties of an inflexion point are that the second differential is zero and that the coefficient undergoes a change in sign on going through such a point. The value of $\theta = \theta_{\text{inf}}$ where θ_{inf} is the orientation corresponding to the point of inflexion in the slowness of erosion curve is given in polar notation when

$$\frac{\mathrm{d}^2[S(0)/S\cos\theta]}{\mathrm{d}^2(\theta)}$$

is zero, i.e. when

$$\frac{\mathrm{d}^2S}{\mathrm{d}\theta^2} = \frac{2}{S}\left(\frac{\mathrm{d}S}{\mathrm{d}\theta}\right)^2 - 2\frac{\mathrm{d}S}{\mathrm{d}\theta}\tan\theta + S(2\sec^2\theta - 1) \qquad (3)$$

S being written for $S(\theta)$. The other two solutions, $S = \infty$ and $\sec\theta = 0$, are meaningless.

Alternatively, if, as in the examples of Carter *et al.* [4], the non-normalized erosion slowness curve, i.e. $(1/S\cos\theta)$, is plotted in the form $1/S$ as a function of $(1/S)\tan\theta$, then the condition for inflexion is

$$\frac{\mathrm{d}^2(1/S)}{\mathrm{d}^2(\tan\theta/S)} = 0 .$$

This relationship holds when

$$\frac{\mathrm{d}^2S}{\mathrm{d}\theta^2} = 2\tan\theta\frac{\mathrm{d}S}{\mathrm{d}\theta} \qquad (4)$$

Analysis of sputter yield curves using the above criteria confirm the existence of an inflexion point to be denoted by θ_{inf}'' in the range $\pm\hat{\theta} < \pm\theta_{\text{inf}}'' < \pm 90^\circ$. As expected, both co-ordinate systems yield the same value for θ_{inf}''. Another inflexion point θ_{inf}' occurs in the region $0 < \pm\theta_{\text{inf}}' < \pm\hat{\theta}$. Construction diagrams reveal that all trajectories are located within the angle enclosing $\text{tr}(\theta_{\text{inf}}')$ and $\text{tr}(\theta_{\text{inf}}'')$. A recent publication by Ducommun *et al.* [6] on an analytical treatment of the development of a general contour under ion etching conditions has noted such points of inflexion and proved the trajectory limitation mathematically. These authors showed that θ_{inf}' and θ_{inf}'' define regions where the evolution process of the surface may be different. Since the present study is concerned with cones with final apex angle of $180^\circ - 2\hat{\theta}$, in Ducommun *et al.*'s notation the data given in this paper are determined in the ranges $\theta_{\text{inf}}' < \hat{\theta}_{\text{m}} < \theta_{\text{inf}}''$ and $\theta_{\text{inf}}' < \hat{\theta} > \theta_{\text{inf}}'' < \theta_{\text{M}}$ where θ_{M} is the maximum slope in the initial profile.

Thirteen sputter yield curves covering as wide a spectrum of experimental conditions as possible have been taken from publications by five different experimenters or groups and studied. It was found that θ_{inf}'' always occurs in the slowness of erosion curve at $\pm\hat{\theta} < \theta_{\text{inf}}'' < \pm\theta^x$. Plotting $\hat{\theta}$ against $100\,(\theta_{\text{inf}}'' - \hat{\theta})/\hat{\theta}$ for $\hat{\theta}$ values between 38° and 80.5° revealed that within experimental error the data points were scattered about a straight line given by

$$\theta_{\text{inf}}'' = \frac{\hat{\theta}}{139}(223 - \hat{\theta}) . \qquad (5)$$

Thus as $\hat{\theta}$ increases θ_{inf}'' approaches $\hat{\theta}$. Since θ_{inf}'' is proportional to $\hat{\theta}$ it will be dependent on the usual ion-bombardment parameters mentioned earlier. The above expression yielded

θ_{inf}'' on average to within 1.7% of the measured value.

One effect of a point of inflexion in the angle range $\hat{\theta}$ to 90° of the slowness of erosion curve is that the statement on orientation trajectories by Carter *et al.* [4] must be slightly modified. All inward drawn normals will have points of intersection for $\theta < \pm \hat{\theta}$, those for $\pm \hat{\theta} < \pm \theta < \pm \theta_{inf}''$ will diverge but intersect with the trajectories for $\pm \theta_{inf}'' < \pm \theta < \pm 90°$ or tr($\pm$ 90°). Investigation of the many Frank constructions done in the present investigation imply that the basic premise that the trajectory corresponding to $\theta = \pm \hat{\theta}$ cannot intersect with any other and thus disappear still stands. The $\pm \hat{\theta}$ trajectory dependence of an equilibrium cone is thus evident, but the profile changes involving the higher angle orientation trajectories will be more complex than previously imagined. The standard structure having its sides exposed all the time to the ion beam means that the converging sides eliminate most of the higher angle trajectories so that the effect of the inflexion point on the resulting profile is minimal for this configuration. The effect would be more pronounced if the sides were exposed gradually with etching time such as for a low sputter yield particle being left proud by the erosion of a high yield surrounding matrix material.

3.3. Spherical target shape

Spheres have practical importance since not only do they frequently appear in a wide variety of materials but considerable experimental work has been carried out by Wehner on the ion bombardment of metal spheres principally by mercury ions [14] and this allows the only available data for comparison with theory known to the author.

Fig. 5 illustrates the variation of sputter yield perpendicular to the target surface with angle of ion incidence for the two different ion-etching situations to be considered here. These conditions are meant to be representative of the extremes of ion etching processes and target shape changes currently employed in surface preparation techniques. The sputter yield values taken from the work of Cheney and Pitkin [16] on 30 keV xenon ion bombardment of a mechanically polished planar copper target show that at higher ion energies the sputter yield peak is at large angles, is narrow and corresponds to a large atom/ion yield. At low energies, represented

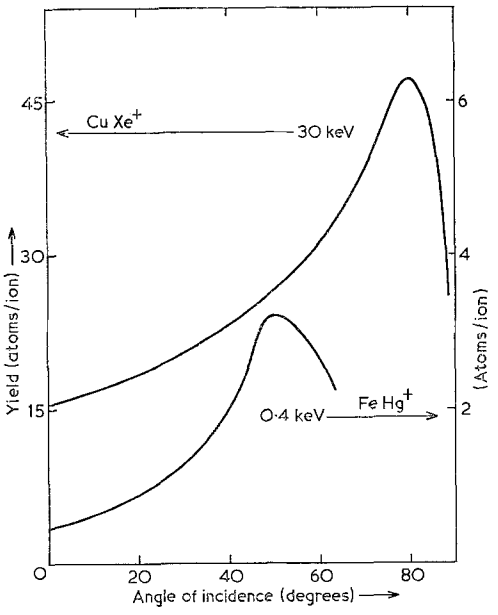

Figure 5 Variation of the sputtering ratio with angle of incidence for Xe^+ 30 keV ions on copper and Hg^+ 0.4 keV ions on iron.

in Fig. 5 by the sputter yield data of Wehner [14] for 0.4 keV Hg^+ ion bombardment of iron, the yield peak is observed to be at smaller angles, broader and corresponds to relatively low yield values. The effects of these two ion-bombarding conditions on the etching of metal spheres are shown in Figs. 6 and 7 where the spheres are represented in two dimensions by circles on polar graph paper. Orientation trajectories are shown every 2° round the circumference except in Fig. 7 where the 47° and 49° trajectories have been added for clarity and those below 28° have been omitted so that the resulting profile is not obscured. The fact that Wehner only gives yield data up to a 60° angle of incidence will not affect discussion of the overall characteristics of resulting etch profiles since the higher angle trajectories are lost early in the process by the restriction caused by the sides of the structure.

The predicted profile changes of the copper sphere caused by high energy ion bombardment are depicted in Fig. 6. It can be seen that the curvature changes of the slowness of erosion curve are relatively small. The orientation trajectories are thus fairly equally spaced resulting in a continuous and smooth change in target profile. While a fairly reasonable cone-shape (pseudo-cone) can be achieved after

most of the sphere has been sputtered away, a pronounced dome-type structure predominates most of the time prior to this. The existence of a dome profile stems from the fact that under these etching conditions, the equilibrium cone angle is small, 20°, so that a considerable quantity of material must be eroded to achieve equilibrium. In contrast, the low energy example (Fig. 7) reveals marked curvature changes in the slowness of erosion curve, non-uniform orientation trajectory spacing and early establishment of a cone-like profile. In this case, trajectories $\mathrm{tr}(\theta) \leqslant \mathrm{tr}(46°)$ are lost before the $0.07d$ etching mark has been realized. The loss of these

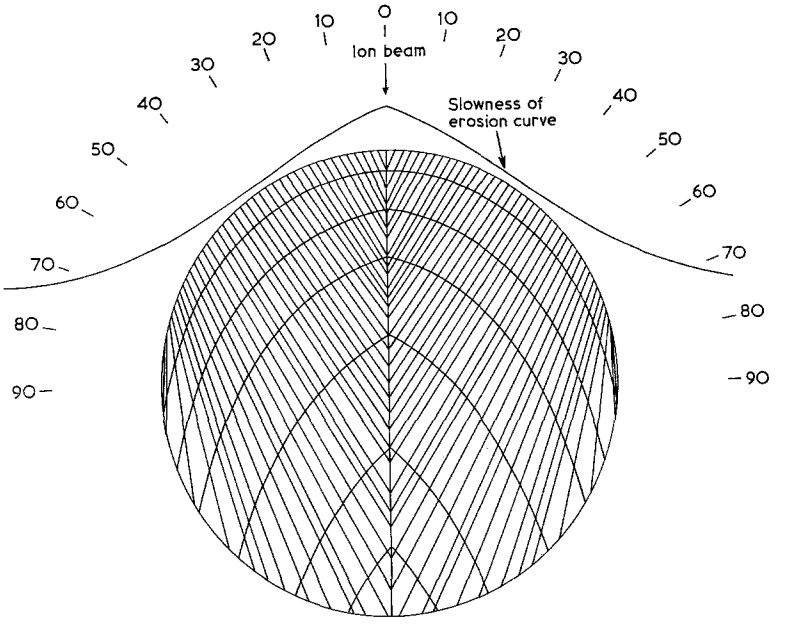

Figure 6 Predicted etching shapes on a copper sphere subjected to ion bombardment by 30 keV Xe^+ ions.

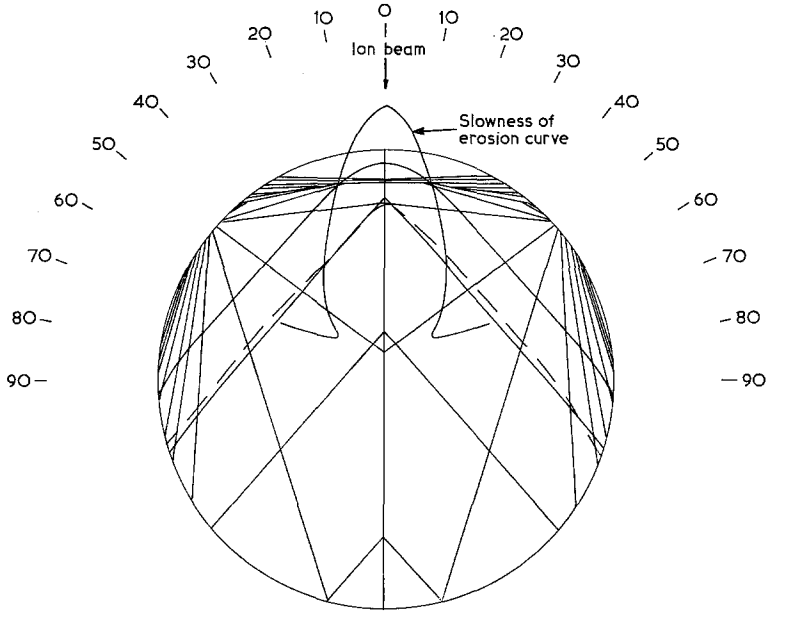

Figure 7 The evolution of sputtered shapes on an iron sphere bombarded by Hg^+ ions at 0.4 keV.

trajectories removes the curvature at the apex angle region so that a point develops on the profile. The overall shape is then essentially governed by the narrow trajectory range corresponding to orientations 46.5° to 50°. Since few trajectories are left to be lost, the structure profile remains almost constant. This narrow orientation range is related directly to the rapid curvature changes in the slowness of erosion curve corresponding to the sputter yield peak. Such an effect is not seen in Fig. 6 since the peak orientations are mostly outside the original sphere surface. In addition, taking the reciprocal of the yield values from curves with peaks having high atom/ion ratios will reduce curvature changes in the area of the slowness of erosion curves corresponding to the peak compared to those erosion curves having lower atom/ion peak values.

After 85% of the diameter of sphere in the direction of the ion beam has been sputtered away, the $0.85d$ mark, the resulting conical shape for the 30 keV case is derived from orientation trajectories 51° to 61° while for the 0.4 keV bombardment example, only orientation trajectories in the very narrow range 48.7° to 49° are involved. Carter *et al.* [4] have pointed out that an equilibrium cone shape can only develop once all trajectories $\mathrm{tr}(\theta) < \mathrm{tr}(\hat{\theta})$ are lost. For copper, Fig. 6, $\hat{\theta}$ is 79.5° and for iron, Fig. 7, 50°. It is thus immediately clear that while Fig. 6 yields a cone angle value of 72° at the $0.85d$ etch mark, this is larger by 52° from the calculated value (Equation 1) because too many lower angle trajectories are present. This also is the cause of the $0.85d$ structure still exhibiting a very slight dome profile. If the initial structure had been of the standard type discussed earlier, the dome profile would have been much more noticeable. It is thus evident that under normal experimental conditions of irregular starting shapes the higher angle orientation trajectories may well not be present so that a non-equilibrium shape can easily be mistakenly classified as equilibrium.

In contrast to the above, the low energy case yields a cone angle of 80°, a value agreeing exactly with calculation. Although the etch structure results from trajectories for orientations less than the sputter yield peak, the trajectory range is so narrow and so close to the peak angle that for a spherical starting shape this is essentially sufficient for equilibrium conditions to apply and result in what one can term a pseudo-cone shape. Under these conditions, very accurate plotting of the sharply changing slowness of erosion curve corresponding to angles immediately either side of the sputter yield peak is of prime importance. Unfortunately, experimentally this part of the sputter yield curve has generally been the least accurately determined.

The validity of the Frank construction process applied to ion-etched structures would seem to be borne out admirably by the dashed curve in Fig. 7. This curve has been obtained by superimposing the outline of an iron sphere etched by 0.4 keV Hg^+ ions from the work of Wehner [14] onto the present diagram. The slight asymmetry is a result of small imperfections in roundness of the starting shape of Wehner's sphere. It was from this outline that the present sputter yield data used in the Frank construction was obtained. Excellent agreement can be seen between the experimentally determined and theoretically predicted etch profile.

In order to indicate how far and how quickly an ion etched sphere's profile might approach an equilibrium cone shape, Frank constructions have been made to the $0.85d$ position, the last profile shown in Figs. 6 and 7, and the apex angle or averaged apex angle in the case of curved sides has been recorded under the column headed "$(\alpha_c)_{FS}$ at $0.85d$" in Tables V and VI. Comparison between these values and the equilibrium values $(\alpha_c)_M$ reveals that in general these cone angles are far from the expected equilibrium values given by $(\alpha_c)_M$. This discrepancy is due solely to the cones being derived from less important orientation trajectories, typically $\mathrm{tr}(\theta)$ where $\theta < \hat{\theta}$. Agreement between "$(\alpha_c)_{FC}$ at $0.85d$" and $(\alpha_c)_M$ to within 5% appears to occur only for heavy ion bombardment at energies $\leqslant 0.8$ keV when the cones are derived from $\mathrm{tr}(\theta)$ orientations where $\theta \approx \hat{\theta}$, such as seen in Fig. 7. Under these experimental conditions, the cone angle is fairly large and will thus appear after relatively little material has been removed. The large Z_1 value for Hg^+ ions also ensures a fairly high normalized sputter yield, $S(\theta)/S(0)$, of the order 3.5 to 7 at the peak [14] compared to 1.5 to 2.5 for the A^+ ion data [11]. While a higher bombardment energy generally increases the sputter yield, it is detrimental since the resulting value of the cone apex angle is considerably reduced so that an equilibrium structure only develops after much more erosion of the original target has taken place. For example, etching copper with xenon ions at 30 keV produces a cone-like structure with apex

TABLE VI

Bombarding ion	Z_1	keV	$(\alpha_c)_M$	$(\alpha_c)_{FC}$ at $0.85d$	$(\alpha_c)_{FR}$				
					at $0.85d$	at $1d$	at $2d$	at $4d$	Ref.
Xe	54	30.0	20	72	NM	NM	26	24	[14]
Ar	18	27.0	24	42	NM	NM	31	29	[15]
Xe	54	9.5	31	66	NM	52	36	35	[14]
Xe	54	1.05	59	77	67	67	65	62	[12]
Kr	36	1.05	49	72	60	58	53	50	[12]
Ar	18	1.05	45	67	54	54	48	45	[12]
He	2	1.05	38	94	62	57	54	41	[12]

Target material Cu ($Z_2 = 29$). NM denotes result not meaningful due to pronounced dome-type structure.

angle 260% greater than the equilibrium value at the $0.85d$ mark while bombarding at 9.5 and 1.05 keV results in much smaller discrepancies of 113% and 32% respectively. As a general rule, it can be stated while a true equilibrium structure cannot be achieved by etching spheres, a pseudo-cone structure appears to be obtainable provided that the ion energy is less than or equal to about 0.5 keV and the incident ion atomic number, Z_1, is large.

In practice, all the rules governing the values and variation of the normalized sputter yield $S(\theta)/S(0)$ are not known at present. The available data on the absolute sputtering ratio $S(\theta)$, in atoms/ion, currently appears to show an increase within a given period of the periodic table as the d shells of the target atoms are filled [11, 19-22]. The influence of the ion through Z_1 and hence M_1 has been noted above. Both Sigmund [23] and Oechsner [11] have reported M_1, M_2 dependences of the sputter yield where M_2 is the mass of the target atom. In the theory due to Sigmund [23] sputtering is assumed to result from cascades of atomic collisions within the target caused by the incident ions while the yield is calculated assuming a random slowing down process in an infinite medium. For $\theta < \hat{\theta}$, Sigmund achieves reasonable agreement within the errors of the experimental results with the relation

$$\frac{S(\theta)}{S(0)} = (\cos\theta)^{-f}.$$

For the elastic collision region f is dependent on the ratio M_2/M_1. For $M_2/M_1 \leqslant 3$, f is about 5/3. The more recent data of Oechsner also imply that the normalized yield is proportional to M_2/M_1. Considering the contribution of particle ejection by a small number of collisions immediately beneath the bombarded surface, he finds for the range 0.55 to 2.05 keV that

$$\frac{S(\hat{\theta})}{S(0)} = \frac{cY - S(0)}{S(0)}$$

where $c = (249 \pm 4)10^{-4}$ and Y is a dimensionless parameter given by $\sigma_1 \epsilon E_0/d^2U_0$, σ_1 is the collision cross-section between the ion and target atom, ϵ is the energy transfer function of the primary collision given by $4M_1M_2/(M_1 + M_2)^2$, d is a statistical average target atom spacing and U_0 is the surface binding or sublimation energy. For small angles of ion incidence, the data yields

$$f \sim \frac{Y}{S(0)}\left(\frac{1}{\hat{\theta}}\right)^2.$$

Oechsner finds that his experimental results lie about one curve similar in shape to a sputter yield curve when

$$\frac{S(\theta) - S(0)}{S(\hat{\theta}) - S(0)}$$

is plotted against $\theta/\hat{\theta}$. For the region $\theta/\hat{\theta} = 0$ to 0.85, the curve is given by

$$\frac{S(\theta) - S(0)}{S(\hat{\theta}) - S(0)} = 1.2\left[\frac{\theta}{\hat{\theta}}\right]^2.$$

3.4. Rod-type structure

The starting shape is very similar to the standard profile described in Sections 2 and 3. In three-dimensions it is a rod with sides parallel to the ion-beam direction. The end of the rod facing the beam is hemispherical. The general shape is indicated by the dashed lines in Figs. 2 and 3. The main differences between the standard and rod structure is that the rod sides place a greater restriction on included orientation trajectories and that since the sides are parallel to the ion beam any particular region on them will not be etched away until the top face has been eroded

down to that region. As a result of the latter, the rod cross-section perpendicular to the beam will remain constant in shape and size with etching time.

The following discussion of ion bombardment of rod structures will be made with reference to Figs. 2 and 3. Comparison between these figures reveals that common to both is the early loss of the higher angle trajectories through the restrictions placed by the structure sides. The important trajectory tr($\hat{\theta}$) is close to the sides of the structure, the degree of proximity increasing with $\hat{\theta}$. As such, the range of trajectories filling the volume between tr($\hat{\theta}$) and the vertical side while being small will decrease with increasing ion energy. For example, for the cases Cu 2.05 keV Xe^+ and Mo 0.2 keV Hg^+ (Figs. 2 and 3), the trajectories filling this volume at a position $0.5d$ correspond to orientations covering about 10°, 7° while at $3d$ it is 1.2°, 0.3°. The reason for the influence and importance of tr($\hat{\theta}$) is thus obvious. This is particularly so in the low energy case for molybdenum since trajectories cover an orientation range between the structure axis and structures sides of less than one degree either side of tr($\hat{\theta}$) at the $3d$ position. The higher energy case has more trajectories between the axis and tr($\hat{\theta}$) and this causes the persistence of the dome profile. This point is emphasized by comparison between the values of $(\alpha_c)_{FR}$ at different axial positions and $(\alpha_c)_M$ (Tables V and VI). A conical shape is achieved sooner for a smaller included trajectory range, that is, lower ion energies and higher Z_1 values.

The elimination of the higher angle trajectories will affect the etching shapes on rod structures compared to those on the standard structure by excluding previous edge areas of the profile. Since these areas generally show considerable curvature, transition from dome-type to a pseudo or true equilibrium condition should occur sooner. To give a rough indication of the change in apex angle by structure side restriction of the enclosed trajectories the angles obtained at the $0.85d$ mark for spheres and rods denoted by $(\alpha_c)_{FC}$ and $(\alpha_c)_{FR}$ respectively are given in Tables V and VI. It must be emphasized that these angles are different from the apex angles listed in Tables I to III in that they are averaged apex angles obtained by drawing two straight lines through the dome profile. It can be seen from these tables that at high ion energies the rod structure profile is too curved for meaningful measurement, but a semi-pseudo conical structure is obtained from the sphere as the latter includes far fewer trajectories. With decreasing ion energy, comparison can reasonably be made between the etch profiles on these structures and this reveals as indicated earlier that close agreement only occurs for low ion energies, under which condition the apex angle is large and the slowness of erosion curve shows sufficient curvature such that the trajectories are widely spaced about tr($\hat{\theta}$).

3.5. Computer simulation

Several computer programs have been written to simulate ion bombardment of surface contours of the form $y = a \sin x$. The first by Catana *et al.* [8] was based on an iteration process and indicated that $\alpha_c = 180° - 2\theta_0$ where $\theta_0 > \hat{\theta}$ and $S(\theta_0) = S(0)$. Corrections to the program by Ishitani *et al.* [9] removed some of the spurious topographical features and produced triangular sections on the surface with slopes near $\hat{\theta}$. This program is obviously still lacking, however, since the profiles show apex angles of 65° to 70° and not the expected 90°. One would anticipate that a symmetrical starting shape, whether it be sinusoidal or any other form, containing orientations $\pm\,\hat{\theta}$ would develop into a cone apex angle of $\alpha_c = 180° - 2\hat{\theta}$. If the structure only contained orientations corresponding to angles $\theta < \hat{\theta}$, then a cone of apex angle $180° - 2\theta'$ should be capable of being produced where θ' would be the angle in the initial structure with the highest sputter yield value. The analytical treatment and non-iterative computer simulation program of Ducommun *et al.* [6] applied to sine-type surfaces show this to occur. In addition their analysis predicts angular points or corners to appear during evolution towards the final ultimate equilibrium state, the horizontal plane. The number of corners is shown to be dependent on the inter-relationship between θ_M, $\hat{\theta}$, θ_{inf}' and θ_{inf}'' for a given set of experimental conditions where θ_M is the maximum value of angle of incidence that the ion beam makes with any part of the initial target profile The profiles on the standard structures agree with their observations in the relevant orientation range.

4. Conclusions

Application of Frank's kinematic theorems of crystal dissolution to the problem of predicting surface topography changes caused by ion bombardment have met with considerable success. Equilibrium cone angles can be deter-

mined on average to within 5%. This compares extremely favourably with the values obtained by calculation. As indicated by Barber *et al.* [1] the main source of error in topography prediction was found to lie with the accuracy of the slowness of erosion curve and hence in the precision of the sputter yield curve. Typically, determinations of the sputter yield with varying angle of ion incidence published in the literature are made only every 5° to 10° so that the drawing of a continuous yield curve might be expected to introduce some if not significant errors. Such discrepancies might be expected to be maximum at the sputter yield peak, the area of the curve exhibiting most curvature change and wielding so much influence on the sputter profiles and cone apex angles through the importance of the orientation trajectories either side of $\mathrm{tr}(\hat{\theta})$. That these errors were not found to greatly affect the cone angle determinations is indicative that the predicted intermediate ion etching shapes should be reasonably precise.

This notion is borne out here by comparisons between Frank constructions applied to Wehner's experimental data on ion etched metal spheres, and from previous work on amorphous materials [1]. It thus appears that the dissolution theorems due to Frank are an extremely powerful technique for describing surface topographic changes during ion bombardment. This applies not only to general surfaces such as described here or as have been demonstrated for InP specimens by Barber *et al.* [1], but also to second phase particles. The proviso must be added, however, that since the theorems were formulated for crystal dissolution by chemical methods they cannot be expected to allow for effects such as ion reflection, surface diffusion, local variations in surface binding energy, redeposition of sputtered material and interference from neighbouring structures. It must be further recognized that crystalline materials can exhibit anisotropic ion-etching effects taking the form of faceting [1, 13, 24, 25]. This occurs through the action of focused collision sequences along rows of nearest or next nearest neighbours [26]. Under this condition, anisotropic slowness of erosion curves must be considered [1]. That this was not necessary to explain Wehner's results is presumably on account of a relatively small grain size compared to the 0.05 cm sphere diameter so that when an averaged grain effect is taken into consideration an isotropic slowness of erosion curve is applicable.

Acknowledgement

The author is indebted to Mrs Peach in the Department of Physics for kindly drawing the diagrams at short notice.

References

1. D. J. BARBER, F. C. FRANK, M. MOSS, J. W. STEEDS and I. S. T. TSONG, *J. Mater. Sci.* **8** (1973) 1030.
2. F. C. FRANK and M. B. IVES, *J. Appl. Phys.* **31** (1960) 1996.
3. F. C. FRANK, *Z. Phys. Chem. Neue Folge* **77** (1972) 84.
4. G. CARTER, J. S. COLLIGON and M. J. NOBES, *J. Mater. Sci.* **8** (1973) 1473.
5. A. D. G. STEWART and M. W. THOMPSON, *ibid* **4** (1969) 56.
6. J. P. DUCOMMUN, M. CANTAGREL and M. MARCHAL, *ibid* **9** (1974) 725.
7. M. J. WITCOMB, *ibid* **9** (1974) 1227.
8. C. CATANA, J. S. COLLIGON and G. CARTER, *ibid* **7** (1972) 467.
9. T. ISHITANI, M. KATO and R. SHIMIZU, *ibid* **9** (1974) 505.
10. M. CANTAGREL and M. MARCHEL, *ibid* **8** (1973) 1711.
11. H. OECHSNER, *Z. Physik* **261** (1973) 37.
12. M. J. WITCOMB, Proceedings of the 11th Annual Conference of the Electron Microscopy Society of Southern Africa, Johannesburg (1972) p. 75.
13. *Idem, J. Mater. Sci.* **9** (1974) 551.
14. G. WEHNER, *J. Appl. Phys.* **30** (1959) 1762.
15. P. SIGMUND, *ibid* **8** (1973) 1545.
16. K. B. CHENEY and E. T. PITKIN, *ibid* **36** (1965) 3542.
17. V. A. MOLCHANOV and V. G. TEL'KOVSKII, *Soviet Phys.-Doklady* **6** (1961) 137.
18. G. D. MAGNUSON, B. B. MECKEL and P. A. HARKINS, *J. Appl. Phys.* **32** (1961) 369.
19. G. K. WEHNER, *Phys. Rev.* **112** (1958) 1120.
20. *Idem, J. Appl. Phys.* **32** (1961) 365.
21. O. E. ALMÉN and G. BRUCE, *Nucl. Instr. Methods* **11** (1961) 257.
22. G. K. WEHNER, *J. Appl. Phys.* **33** (1962) 1842.
23. P. SIGMUND, *Phys. Rev.* **184** (1969) 383.
24. G. K. WEHNER, *ibid* **102** (1956) 690.
25. I. H. WILSON and M. W. KIDD, *J. Mater. Sci.* **6** (1961) 1362.
26. R. S. NELSON and M. W. THOMPSON, *Proc. Roy. Soc.* **A259** (1961) 458.

Received 29 August and accepted 9 September 1974.